**Supporting Information Cover Sheet**

# Adsorption of Tetracycline and Sulfamethoxazole on Crop Residue-derived Ashes: Implication for the Relative Importance of Black Carbon to Soil Sorption

Liangliang Ji[1,2], Yuqiu Wan[1], Shourong Zheng[1], and Dongqiang Zhu[1]*

[1]State Key Laboratory of Pollution Control and Resource Reuse and School of the Environment, Nanjing University, Jiangsu 210093, China

[2]Key Laboratory of Integrated Regulation and Resource Development on Shallow Lakes, Ministry of Education and College of Environmental Science and Engineering, Hohai University, Nanjing, 210098, China

Submitted to *Environmental Science & Technology*

Prepared on *February 12*, *2011*

Number of pages: 10
Number of tables: 4
Number of figures: 5

**Table S1.** Summary of Sorbate Properties (Water Solubility–$S_W$, *n*-Octanol-water Partition Coefficient–$K_{OW}$, and Acidity Dissociation Constant–p$K_a$).

| **Compound** | **Molecular weight** | $S_W$ **(mmol/L)** | log $K_{OW}$ **(L/L)** | p$K_a$ |
|---|---|---|---|---|
| sulfamethoxazole | 253.28 | 1.46 [a] | 0.890 [b] | 1.8(1), 5.6(2) [b] |
| tetracycline | 444.43 | 3.8 [c] | -1.19 [c] | 3.30(1), 7.68(2), 9.69(3) [c] |

[a] From Pérez et al. (*1*). [b] From Gao et al. (*2*). [c] From Tolls (*3*).

**References**


1. Pérez, S.; Eichhorn, P.; Aga, D. S. Evaluating the biodegradability of sulfamethazine, sulfamethoxazole, sulfathiazole, and trimethoprim at different stages of sewage treatment. *Environ. Toxicol. Chem*. **2005**, 24, 1361–1367.
2. Gao, J. A.; Pedersen, J. A. Adsorption of sulfonamide antimicrobial agents to clay minerals. E*nviron. Sci. Technol*. **2005**, 39, 9509–9516.
3. Tolls, J. Sorption of veterinary pharmaceuticals in soils: A review. *Environ. Sci. Technol*. **2001**, 35, 3397–3406.

**Table S2.** Surface Elemental Composition (on a Dry Weight Basis) Determined by X-ray Photoelectron Spectroscopy (XPS) for Raw and Acid-treated Wheat-residue-derived Black Carbon (wBCraw and wBCacid) and Maize-residue-derived Black Carbon (mBCraw and mBCacid).

| **Adsorbent** | **Surface elemental composition** [a] | | | | | |
|---|---|---|---|---|---|---|
| | **N%** | **P%** | **Mg%** | **Al%** | **K%** | **Ca%** |
| wBCraw | BDL [b] | BDL [b] | BDL [b] | BDL [b] | 5.29 | 0.92 |
| wBCacid | 0.66 | 0.50 | BDL [b] | BDL [b] | BDL [b] | BDL [b] |
| mBCraw | BDL [b] | 0.91 | 6.69 | BDL [b] | 2.04 | 1.35 |
| mBCacid | 1.35 | 0.30 | BDL [b] | 1.63 | BDL [b] | BDL [b] |

[a] Elemental content of C, O, Si is presented in Table 1 in the main text. [b] Below detectable level.

**Table S3.** Mineral composition (on a Dry Weight Basis) Determined by X-ray Fluorescence (XRF) for Raw and Acid-treated Wheat-residue-derived Black Carbon (wBCraw and wBCacid) and Maize-residue-derived Black Carbon (mBCraw and mBCacid).

| **Adsorbent** | **Component** | | | | | | |
|---|---|---|---|---|---|---|---|
| | **$SiO_2$%** | **MgO%** | **CaO%** | **$K_2O$%** | **$P_2O_5$%** | **$Fe_2O_3$%** | **$Al_2O_3$%** |
| wBCacid | 0.06701 | 0.0614 | 0.00844 | 0.00303 | 0.00262 | 0.00229 | BDL [a] |
| wBCraw | 24.59232 | 0.39211 | 0.38809 | 0.4218 | 0.1497 | 0.1495 | 0.06879 |
| mBCacid | 13.40252 | 0.53106 | 0.11564 | 0.31937 | 0.02846 | 0.16864 | 3.00098 |
| mBCraw | 36.15281 | 6.03643 | 4.17368 | 2.63932 | 4.25876 | 0.74514 | 4.34125 |

[a] Below detectable level.

**Table S4.** Summary of Freundlich Model Parameters ($K_F$ and $n$ ± Standard Deviation) and Distribution Coefficient ($K_d$) for Sorption to Raw and Acid-treated Wheat-residue-derived Black Carbon (wBCraw and wBCacid) and Maize-residue-derived Black Carbon (mBCraw and mBCacid), Bulk Soil, and $Na^+$-saturated Montmorillonite.

| **Compound** | **Adsorbent** | $K_F$ **(mmol$^{1-n}$ L/kg)** | $n$ | $R^2$ | $K_d$ [a] **(L/kg)** |
|---|---|---|---|---|---|
| sulfamethoxazole | wBCraw | 160±10 | 0.28±0.01 | 0.987 | 10500 |
| | wBCraw/DSHA [e] | 116±7 | 0.32±0.01 | 0.988 | 6030 |
| | wBCacid | 570±20 | 0.266±0.008 | 0.991 | 40500 |
| | mBCraw | 32±2 | 0.294±0.008 | 0.992 | 1930 |
| | mBCraw/DSHA [e] | 28±3 | 0.40±0.02 | 0.978 | 914 |
| | mBCacid | 200±8 | 0.229±0.008 | 0.987 | 17600 |
| | bulk soil | 50±30 | 1.4±0.1 | 0.962 | 4.90 |
| | $Na^+$-montmorillonite | 0.9±0.3 | 0.86±0.05 | 0.961 | 2.03 |
| tetracycline | wBCraw | 790±80 | 0.39±0.02 | 0.971 | 27300 |
| | wBCraw/DSHA [e] | 1200±100 | 0.49±0.02 | 0.979 | 23200 |
| | wBCacid | 1210±50 | 0.237±0.009 | 0.984 | 102000 |
| | mBCraw | 1700±100 | 0.55±0.02 | 0.990 | 23200 |
| | mBCraw/DSHA [e] | 3900±700 | 0.71±0.04 | 0.971 | 21000 |
| | mBCacid | 660±50 | 0.25±0.01 | 0.957 | 17600 |
| | bulk soil | 60±3 | 0.21±0.01 | 0.959 | 5910 |
| | $Na^+$-montmorillonite | 420±20 | 0.32±0.01 | 0.992 | 21800 |

[a] Calculated from the Freundlich model at an equilibrium aqueous concentration ($C_e$) of 0.003 mmol/L. The selected $C_e$ was located approximately in the middle of the isotherm concentration ranges.

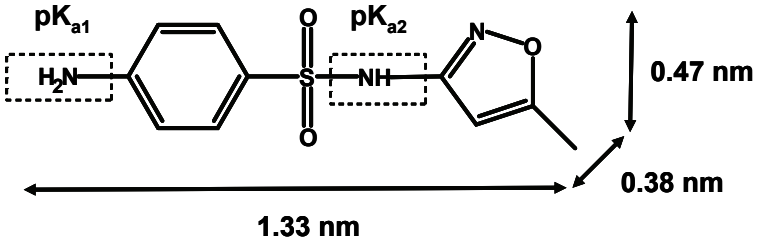


Sulfamethoxazole (SMX)

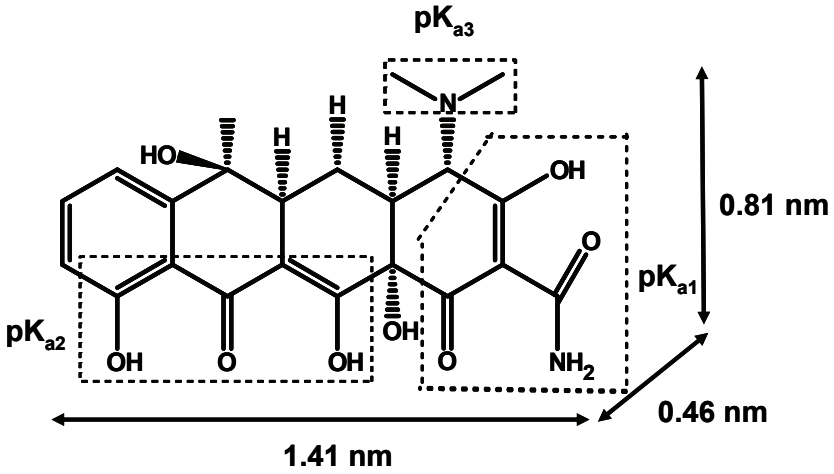


Tetracycline (TC)

**Figure S1.** Chemical structures and molecular sizes of sulfamethoxazole and tetracycline. The regions framed by dashed lines represent the structural moieties associated with the acidic dissociation constants (p$K_a$) (values shown in Table S1).

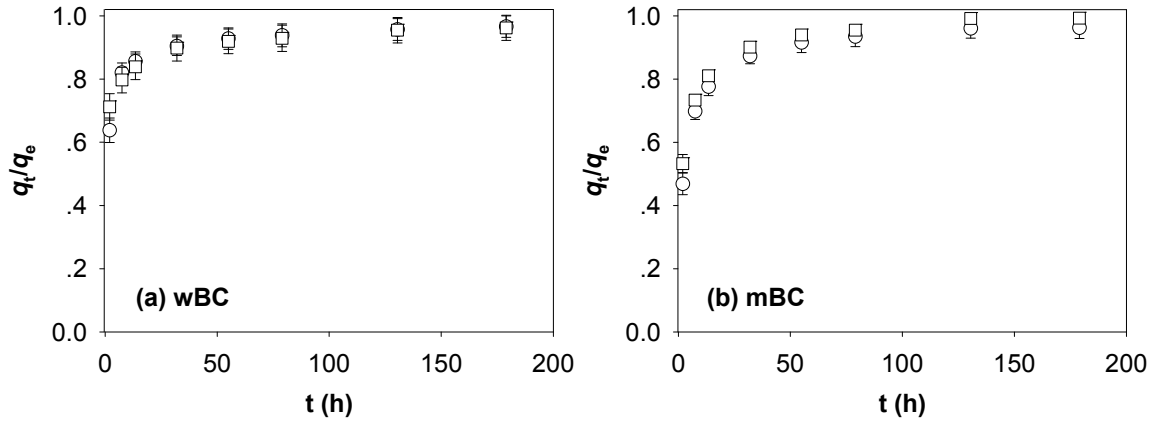


**Figure S2.** Adsorption kinetics of sulfamethoxazole plotted as ratio of adsorbed concentration ($q_t$) at a given time ($t$) to equilibrium adsorbed concentration ($q_e$) on different adsorbents. (a) Wheat-residue-derived black carbon (wBC). (b) Maize-residue-derived black carbon (mBC). ○ = raw sample; □ = acid-treated sample. Error bars represent standard deviations calculated from triplicate samples.

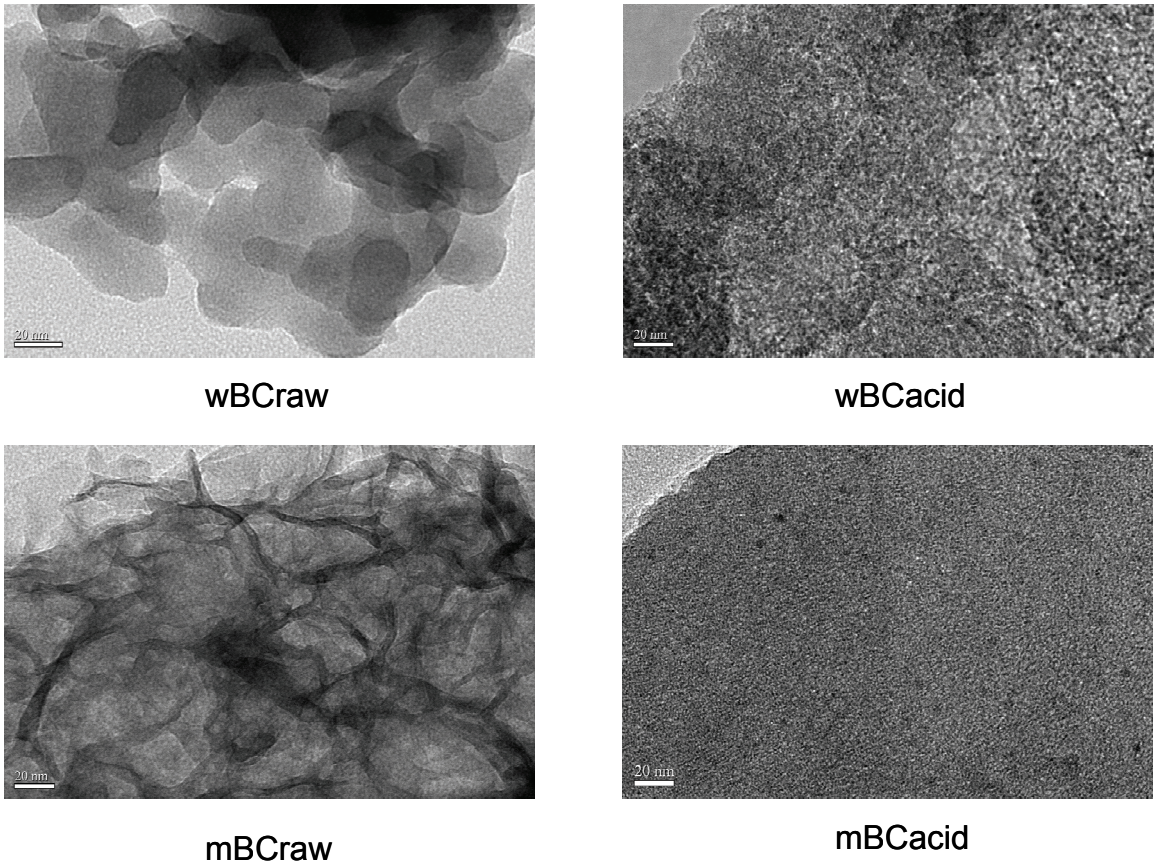


**Figure S3.** Transmission electron microscopy (TEM) images of raw and acid-treated wheat-residue-derived black carbon (wBCraw and wBCacid) and maize-residue-derived black carbon (mBCraw and mBCacid).

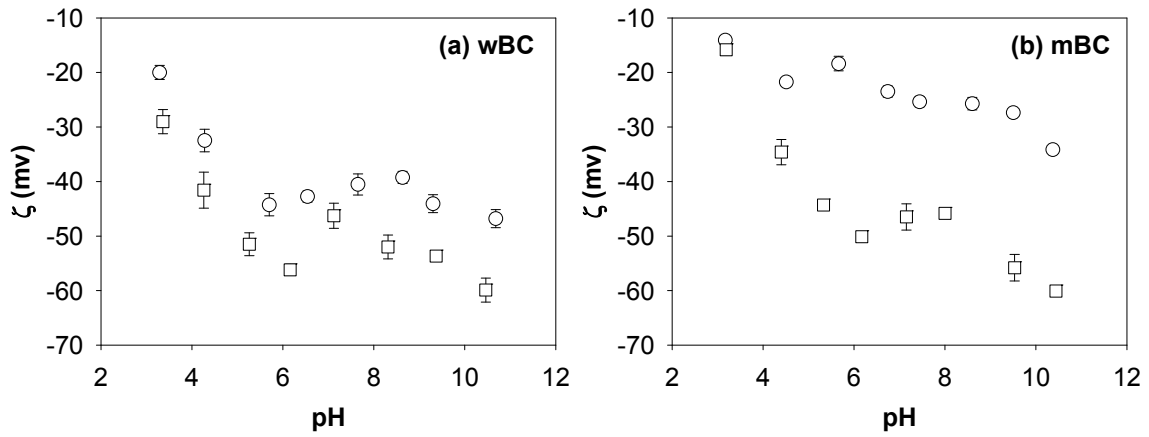


**Figure S4.** Zeta potential (ζ) as a function of pH. (a) Wheat-residue-derived black carbon (wBC). (b) Maize-residue-derived black carbon (mBC). ○ = raw sample; □ = acid-treated sample.

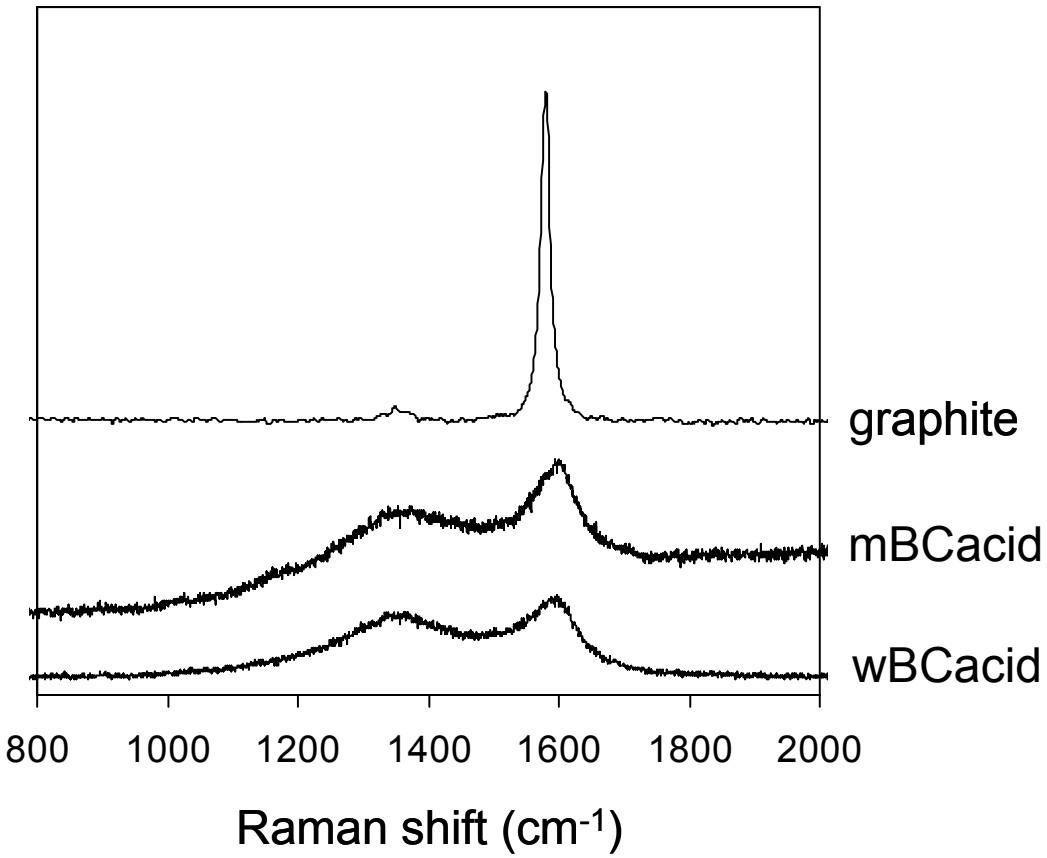


**Figure S5.** Raman spectra of acid-treated wheat-residue-derived black carbon (wBCacid) and maize-residue-derived black carbon (mBCacid) and nonporous pure graphite. All samples display strong Raman peaks around 1336 and 1590 $cm^{-1}$, assigned to the D band and the G band, respectively. The G band is characteristic of the stretching vibration of carbon $sp^2$ bonds in a two-dimensional hexagonal lattice, while the D band is characteristic of the vibration of carbon atoms with dangling bonds in an amorphous carbon network (*1*). It is thus demonstrated that the graphitized carbon in wBCacid and mBCacid has lower structural order than pure graphite.

**References**

1. Paredes, J. I.; Villar-Rodil, S.; Solis-Fernandez, P.; Martinez-Alonso, A.; Tascon, J. M. D. Atomic force and scanning tunneling microscopy imaging of graphene nanosheets derived from graphite oxide. *Langmuir* **2009,** *25,* 5957–68.